

Geophysical Research Letters®

RESEARCH LETTER

10.1029/2024GL112476

Yan Zhou and Steven Franke contributed equally to this work

Key Points:

- Subglacial channels near the grounding zone are stable in space but toggle activity within decades
- Ice-shelf channel morphology identifies one water outlet as active for hundreds of years before it shut down 60 years ago
- Radio-echo sounding documents the reactivation of a subglacial channel within eight years near the grounding zone

Supporting Information:

Supporting Information may be found in the online version of this article.

Correspondence to:

S. Franke,
steven.franke@awi.de

Citation:

Zhou, Y., Franke, S., Kleiner, T., Drews, R., Humbert, A., Jansen, D., et al. (2025). Reactivation of a subglacial channel around the grounding zone of Roi Baudouin Ice Shelf, Antarctica. *Geophysical Research Letters*, 52, e2024GL112476. <https://doi.org/10.1029/2024GL112476>

Received 12 SEP 2024

Accepted 18 DEC 2024



Author Contributions:

Conceptualization: Reinhard Drews, Olaf Eisen
Data curation: Yan Zhou, Steven Franke, Thomas Kleiner, Daniela Jansen, Daniel Steinhage
Formal analysis: Yan Zhou, Steven Franke, Reinhard Drews
Funding acquisition: Yan Zhou, Steven Franke, Reinhard Drews, Olaf Eisen
Investigation: Yan Zhou, Steven Franke, Thomas Kleiner, Reinhard Drews, Angelika Humbert, Daniela Jansen, Daniel Steinhage, Olaf Eisen

© 2025. The Author(s).

This is an open access article under the terms of the [Creative Commons Attribution License](#), which permits use, distribution and reproduction in any medium, provided the original work is properly cited.

Reactivation of a Subglacial Channel Around the Grounding Zone of Roi Baudouin Ice Shelf, Antarctica

Yan Zhou^{1,2,3} , Steven Franke^{1,4} , Thomas Kleiner¹ , Reinhard Drews⁴ , Angelika Humbert^{1,5} , Daniela Jansen¹ , Daniel Steinhage¹ , and Olaf Eisen^{1,5} 

¹Alfred Wegener Institute Helmholtz Centre for Polar and Marine Research, Bremerhaven, Germany, ²College of Construction Engineering, Jilin University, Changchun, China, ³Polar Research Institute of China, Shanghai, China, ⁴Department of Geosciences, Tübingen University, Tübingen, Germany, ⁵Department of Geosciences, University of Bremen, Bremen, Germany

Abstract Subglacial water beneath the Antarctic Ice Sheet is often funneled via subglacial channels, which inject freshwater into ice-shelf cavities where it interacts with ocean water. The temporal variability of this system has been poorly observed, but its importance for ice dynamics is well recognized. Airborne radar data show a subglacial channel evolving within a decade near of the grounding zone of the Roi Baudouin Ice Shelf (East Antarctica), while topographic signatures on the ice shelf indicate prior inactivity for 60 years. Combining our observations with subglacial hydrological modeling, we suggest that the interplay between episodic subglacial water pulses and ocean water intrusion drive the opening and closing of the channels. Our findings illuminate the short-term transient nature of subglacial channel activity. This impacts ice-shelf–ocean processes, which are important for constraining increasing ocean warming onto ice-shelf basal mass balance, but pose significant challenges for subglacial hydrological modeling at the grounding zone.

Plain Language Summary This study explores how water moves under the ice in Antarctica and how it interacts at the ice–ocean boundary. Using radar, we studied a part of the Roi Baudouin Ice Shelf in East Antarctica and found that water channels under the ice have changed significantly over the last decades. The radar images from 2011 to 2019 showed that these channels open and close within a decade, likely due to changes in water supply from the inland and intrusion of ocean water. This means that the water flow under the ice is not steady, influencing melting at the underside and affecting its movement. These discoveries show that the subglacial water system under Antarctic Ice Sheet is more complicated, making it harder to project future changes in sea-level rise and the effects of climate change on the polar regions.

1. Introduction

Antarctica's ice mass loss primarily originates from the flow of ice from its interior toward the grounding zone, where it meets the ocean (Rignot & Steffen, 2008) and is expected to significantly contribute to future sea-level rise (Edwards et al., 2021). The grounding zone represents a region where the grounded ice sheet transitions into the freely floating ice shelf, typically over several kilometres where the grounding line is slightly moving with tides (Parizek, 2024). The floating ice shelves represent the seaward extensions of the Antarctic ice sheet, which critically influence ice flow by impeding ice discharge into the ocean, particularly at pinning points (Dupont & Alley, 2005; Fürst et al., 2016). This buttressing effect significantly regulates Antarctica's mass loss (Favier et al., 2016; Reese et al., 2018), and, hence, sea-level contribution, emphasizing the importance of understanding the interplay between ice shelves, ocean, atmosphere, and grounded ice sheet.

One of the principal mechanisms contributing to ice-shelf disintegration and subsequent reduction in effective buttressing is melting at the ice-shelf base (van der Linden et al., 2023). This process is predominantly driven by oceanic circulation patterns below the ice shelf within the ice-shelf cavity, generating warm meltwater plumes (Holland et al., 2007; Jenkins, 1991). Next to the overall ice-shelf mass loss due to basal melting, along-flow oriented basal channels develop in localized regions of enhanced basal melting, leaving distinctive curvilinear imprints on the ice-shelf surface (Alley et al., 2016; Drews, 2015; Drews et al., 2020; Gourmelen et al., 2017; Rignot & Steffen, 2008). These ice-shelf channels are critical in ice-shelf stability and freshwater input to the surrounding ocean via the ice-shelf cavity (Alley et al., 2016; Cheng et al., 2024; Gourmelen et al., 2017).

Methodology: Yan Zhou, Steven Franke, Thomas Kleiner, Reinhard Drews, Angelika Humbert, Olaf Eisen
Project administration: Olaf Eisen
Software: Steven Franke, Thomas Kleiner, Angelika Humbert
Supervision: Steven Franke, Olaf Eisen
Validation: Yan Zhou, Steven Franke, Thomas Kleiner
Visualization: Yan Zhou, Steven Franke
Writing – original draft: Yan Zhou, Steven Franke
Writing – review & editing: Steven Franke, Thomas Kleiner, Reinhard Drews, Olaf Eisen

While subglacial channels are primarily sustained and deepened by meltwater plumes away from the grounding zone, the initial formation of these channels remains subject to multiple hypotheses. Notably, many subglacial channels align with locations where modeled subglacial water passes the grounding zone and leaves the grounded ice sheet (Drews et al., 2017; Humbert et al., 2022; Le Brocq et al., 2013; Marsh et al., 2016). Here, fresh subglacial water meets ocean water, giving rise to and entraining warmer ocean water, which induces larger localized sub-ice-shelf melt rates. This can lead to the formation of water-filled cavities, sometimes hundreds of meters high, reaching several kilometres landwards of the continental grounding zone (Whiteford et al., 2022). High wall-melting rates maintain the cavity by preventing cavity closure through upstream ice advection (Drews et al., 2017). Models coupling ice flow and subglacial channelized drainage produce channels which are increasing in cross-sectional area by an order of magnitude through high-effective pressure upstream of the grounding zone (Lu & Kingslake, 2024). However, even though the principal physical mechanism for this type of channel formation is known, the spatial and temporal dynamics of such subglacial hydrological activities and their interactions with the ocean pose significant challenges for characterization, resulting in a limited understanding of these processes.

In this study, we investigate the temporal dynamics of subglacial channel activity at and upstream of the grounding zone of the Roi Boudouin Ice Shelf (RBIS). We utilize time slices of airborne radar data collected in 2011 and 2019, which provide insight into the internal structure of the ice sheet. Additionally, we analyze morphological structures on the surface of the ice shelf. A comparison of radar repeat flights over the grounded ice sheet around the grounding zone suggests that englacial features, which we interpret as oversized subglacial channels, have undergone significant temporal changes over an eight-year period. Ice-shelf channels further seawards are an archive for the location of the subglacial water outlet providing evidence for both spatial stability over hundreds of years and temporal toggling of the outlet activity.

2. Data and Methods

2.1. Radar Data Acquisition and Processing

We used airborne radar data collected with two different radar systems by AWI (Alfred-Wegener-Institut Helmholtz-Zentrum für Polar- und Meeresforschung, 2016) to map englacial reflections in the vicinity of the grounding zone of East Antarctica's Roi Boudouin Ice Shelf. The radar profiles are oriented orthogonally to ice flow and roughly parallel to the grounding zone and cover both the grounded part of the ice sheet as well as the ice shelf (Figure 1).

In austral summer of 2018/19, we acquired multi-channel ultra-wideband (UWB MCoRDS 5 system) radar data (Hale et al., 2016; Rodriguez-Morales et al., 2014) in a frequency range of 150–520 MHz. The radar consisted of an eight-element antenna array mounted on AWI's Polar 6 BT-67 aircraft (Alfred-Wegener-Institut Helmholtz-Zentrum für Polar- und Meeresforschung, 2016) during the CHIRP DML survey (Channel and Ice Rise Project in DML). Data acquisition consisted of staged linear modulated chirp signals (1 μ s unamplified, 1 μ s high-gain and 3 μ s high-gain) to sound the entire ice column at high resolution (Koch et al., 2023). For radar data processing, we used the Open Polar Radar Toolbox (Open Polar Radar, 2023) and applied pulse compression, synthetic aperture radar (SAR) processing, motion compensation, and array processing (Franke et al., 2021, 2022; Leuschen et al., 2000; Rodriguez-Morales et al., 2014). The data product has a range resolution of \sim 0.35 m and an along-track trace spacing of \sim 15 m. The UWB data set comprises five profiles, where four are located a few kilometers upstream of the grounding zone with a profile spacing between 1.5 and 3 km. The fifth profile is located \sim 12 km downstream of the grounding zone on the ice shelf (Figure 1).

In addition, we use radar data acquired in January 2011 with AWI's airborne Electromagnetic Reflection (EMR) system (Nixdorf et al., 1999). These data have been used in previous studies (Callens et al., 2014; Drews et al., 2017), and we use them here to monitor temporal changes that have occurred since. The Aero-EMR operates with a 150 MHz 60 ns burst transmit signal. The recorded radar signals were amplified, band-pass filtered, and passed on to an analog-digital converter. Moreover, the radar data were stacked ten-fold along-track to improve the signal-to-noise ratio. The EMR-60 ns data product has a range resolution of \sim 5.6 m and an along-track trace spacing of \sim 60–100 m.

In this study, we considered four radar profiles, which are mostly located at and upstream of the grounding zone and have a profile spacing of \sim 13 km. The northernmost EMR radar profile overlaps with one of the UWB

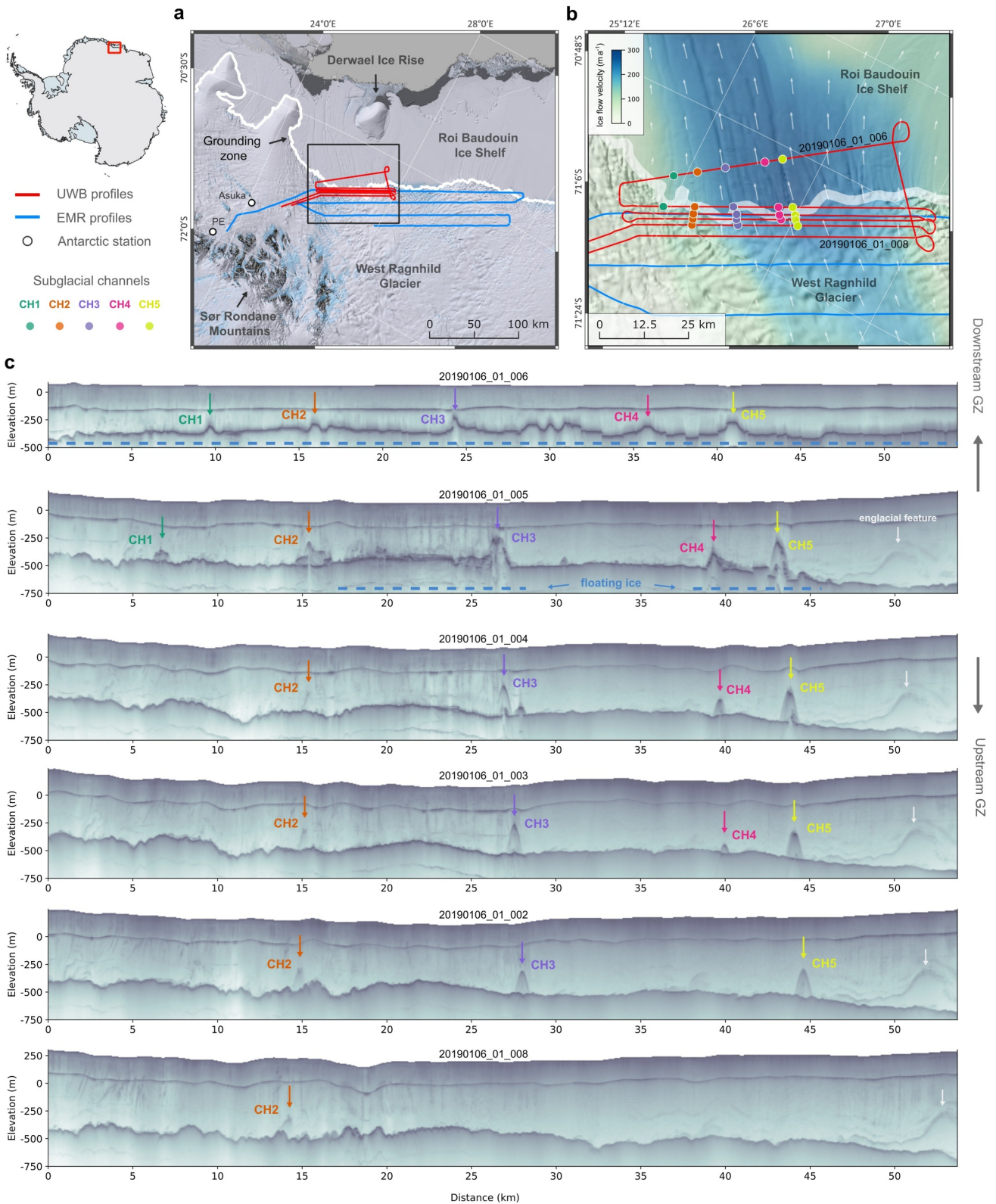


Figure 1. Survey region and overview of radar features. (a) Coastal eastern Dronning Maud Land with radar survey lines with color coding as indicated in the legend. (b) Magnified view on the survey region with ice-flow velocity (Mouginot et al., 2019) in the background. (c) UWB radargrams from North to South (ice flow from bottom to top), with annotations highlighting distinct englacial features discussed in the text. Numbers on top indicate profile labels for unique identification and are also indicated in (b) The grounding zone (Mouginot et al., 2017) in (b) is indicated as a white band.

profiles close to the grounding zone. The southernmost EMR profile is located ~ 45 km upstream of the grounding zone (Figure 1). For conversion from time to depth domain for all radar data we used a constant relative dielectric permittivity value of 3.15 for ice, which corresponds to an electromagnetic wave speed of $1.689 \cdot 10^8$ m s⁻¹.

2.2. Ice Surface Elevation, Bed Topography and Flow Velocity

We used the ice surface elevation, bed topography, and ice surface flow velocity data to explore the englacial features in the radar data, using the ice surface and subglacial topography signatures. Ice surface topography was obtained from the Reference Elevation Model of Antarctica (REMA) digital elevation model (DEM) and resampled to a resolution of 8 m (Howat et al., 2019). Based on the surface DEM we created a hillshade to detect the imprint of subglacial channels in the ice surface. For bed topography, we use BedMachine Antarctica v3 (Morlighem et al., 2020) with a resolution of 500 m. In addition, we used the Antarctic-wide ice surface flow velocity product from Mouginot et al. (2019) to calculate the advection time and distance of ice surface features.

2.3. Subglacial Hydrology Modeling

We applied subglacial hydrological modeling in the drainage basin feeding into RBIS to explore the linkage between subglacial water and the features in our RES and remote sensing data. We used the MPI parallel version of the Confined-Unconfined Aquifer System model (CUAS-MPI; Beyer et al., 2018; Fischler et al., 2023), which can represent the physics of a distributed and channelized subglacial hydrological system over a large area and in high temporal resolution. The model uses a single-layer equivalent porous medium approach, which solves a two-dimensional Darcy-type groundwater flow equation, accounting for spatially and temporally evolving hydraulic transmissivity and taking into account both confined and unconfined aquifer conditions (Beyer et al., 2018; Fischler et al., 2023). The model adopts the classical channel equations (Nye, 1976; Röthlisberger, 1972) as in de Fleurian et al. (2016) and cavity opening (Kamb, 1987; Walder, 1986) as in Werder et al. (2013) to evolve the effective transmissivity. For further details see Supplementary Text S1 in Supporting Information S1.

In addition, we applied the CiDRE (Cordial Drainage Routing Engine) model (Beyer, 2020) to generate subglacial water propagation pathways and flow accumulation based on the hydropotential (Shreve, 1972) and subglacial water routing following the methods outlined by Schwanghart and Kuhn (2010). To account for uncertainties in the input data sets (e.g., ice thickness and ice surface elevation), we follow Neckel et al. (2021) and consider the uncertainty estimates of both data sets. The uncertainty limits were based on the information given by the specific data sets and range from ± 2.4 m in ice surface elevation (Howat et al., 2019) and 10–1,000 m for ice thickness (Morlighem et al., 2020). We conducted 1,000 calculations of subglacial routing pathways, adding a random error to both input data sets within the uncertainty limits, and stacked the results to provide a comprehensive range of potential water routing pathways.

3. Results

3.1. Englacial Channels in Radar Data

Our UWB radar data from 2019 detected strong englacial reflections in the vicinity of the grounding zone at the RBIS (Figure 1). Upstream of the grounding zone they appear as cone-shaped events with pronounced point-like reflections at their apex, which reoccur systematically along the subglacial channels across individual radar profiles (Figure 1c). At the grounding zone and on the ice shelf, we generally observe broader, step-like event signatures following the reflection of the ice base.

These reflections are observed up to more than 5 km upstream of the grounding zone, within a similar distance (traveltime) range in the radargrams. Therefore, we rule out that these could be off-nadir reflections from seawater-filled channels on the ice shelf or at the grounding zone (Jeofry et al., 2018), as the radar's beam angle does not permit to detect reflections from such a distance at angles up to three times larger as its beam angle of $\sim 21^\circ$ in sounding mode (Franke et al., 2022). Moreover, the off-nadir reflections would appear in a much higher range in the nadir-projected signal in the radargrams (approximately at 3 km depth; see Supplementary Text S2 in Supporting Information S1). It is possible that the reflections may consist of a more complex signal that includes off-nadir reflections from the immediate vicinity within a few tens to hundred meters radius (Jacobel et al., 2014). However, the recurring signal along the radar profiles at similar locations and similar range suggests that this is an englacial reflector on the grounded part of the ice sheet, extending parallel to the flow direction.

Based on their spatial positioning and geometrical attributes within the radargrams, we categorize these reflections into coherent features designated as subglacial channels (CH1–CH5). Three of these subglacial channels (CH3–CH5) were reported in previous surveys (Drews et al., 2017). We consider two possible configurations for these channels that could produce the observed reflections: (a) they are water-filled cavities, several hundred meters high and a few tens to hundreds of meters wide, similar to those observed by Whiteford et al. (2022); Horgan et al. (2023); Fox (2023) at the Kamb Ice Stream and potentially filled with sedimentary material (Drews et al., 2017); (b) they are smaller subglacial channels that have a vertical crevasse on their upper side (Vaughan et al., 2012).

The UWB profile at the grounding zone from 2019 overlaps with an EMR profile acquired in 2011 (Figure 2). A detailed comparison shows that the size and shape of some of these cavities have changed close to the limits of the radar resolution. Two additional smaller channel signatures between CH4 and CH5 are evident in the 2011 EMR profile but not visible in the 2019 UWB profile. Most importantly, CH2 is completely absent in the 2011 EMR profile (Figures 2c and 2d). In the UWB data, the cavity of CH2 is vertically incised by about 190 m with respect to the surrounding ice-sheet bed reflection.

The subglacial channels exhibit variations in both spatial extent and radar backscattering characteristics. On the grounded part near the grounding zone, some channels (CH3–5 in profile 20190106_01_004) exhibit gaps in the basal reflection. Further upstream, however, a continuous basal reflection is observed, which could be explained by the channels becoming narrower and the radar return additionally being influenced by side reflections. The westernmost channel (CH1) appears solely at the grounding zone and on the ice shelf and has the lowest height above the surrounding ice-sheet base. Channels CH3, CH4, and CH5 are distinctly observable on the shelf and extend up to approximately 10 km upstream of the grounding zone in our UWB data set. The height of CH4 exhibits a gradual increase with advection across the grounding zone, whereas CH3 and CH5 remain above 200 m height (Supplementary Figure S2 in Supporting Information S1). For these three channels, we also observe an increase in return power with decreasing distance toward the grounding zone. CH2 is clearly visible in the two northernmost profiles (at the grounding zone and on the ice shelf). Its radar signature upstream of the grounding zone is less distinct and weaker compared to the other channels, therefore we speculate if the reflection could present the tip of a vertical crevasse (Vaughan et al., 2012) above a smaller subglacial conduit. Furthermore, CH2 is the only channel identifiable in the southernmost radar profile.

In addition to radar reflections from the subglacial channels, a distinct layer-like englacial reflector is located at the eastern edge of the profiles. This reflection does not follow the bed topography and does not exhibit a resemblance to the signatures of CH1–5. Instead, it resembles the shape of an anticline, with a wavelength of ~ 5 km and an elevation of roughly ~ 300 m and could be an indication of large-scale englacial folding providing insights into the mechanical properties of the ice (Zhang et al., 2024). However, this reflection is not apparent in the radar profile on the ice shelf.

3.2. Channel Imprint on the Ice-Shelf Surface

Downstream of the grounding zone, we observe typically elongated surface troughs on the ice shelf in alignment with the flow direction, which coincide with the locations of identified subglacial channels in the radar data. These troughs start at the grounding zone for CH1, CH3, CH4, and CH5 and some of these surface features exhibit deviations from flowlines discussed elsewhere (Alley et al., 2024; Drews et al., 2020). However, CH2 presents a different pattern: its surface depression is nearly absent up to approximately 10 km downstream of the grounding zone (Figure 2e). Moreover, the location where the surface trough becomes clearly visible corresponds to a deeper, topographically confined elliptical depression. This depression was investigated previously and tentatively interpreted as an englacial lake (Berger et al., 2017), advected from the grounding zone area (Supplementary Figure S3 in Supporting Information S1) where surface melting frequently occurs (Lenaerts et al., 2017).

3.3. Subglacial Hydrology Modeling

The CUAS-MPI simulations (Supplementary Figures S4 a–S4d in Supporting Information S1) lead to a small band close to the grounding zone with low effective pressure ($N = p_{\text{ice}} - p_{\text{water}} \approx 0$ MPa) that is primarily caused by the applied ocean boundary condition. In this band, the high effective transmissivity ($T_{\text{eff}} > 1 \text{ m}^2 \text{ s}^{-1}$) would allow for efficient water transport. Since the water input into the model originates from geothermal heat

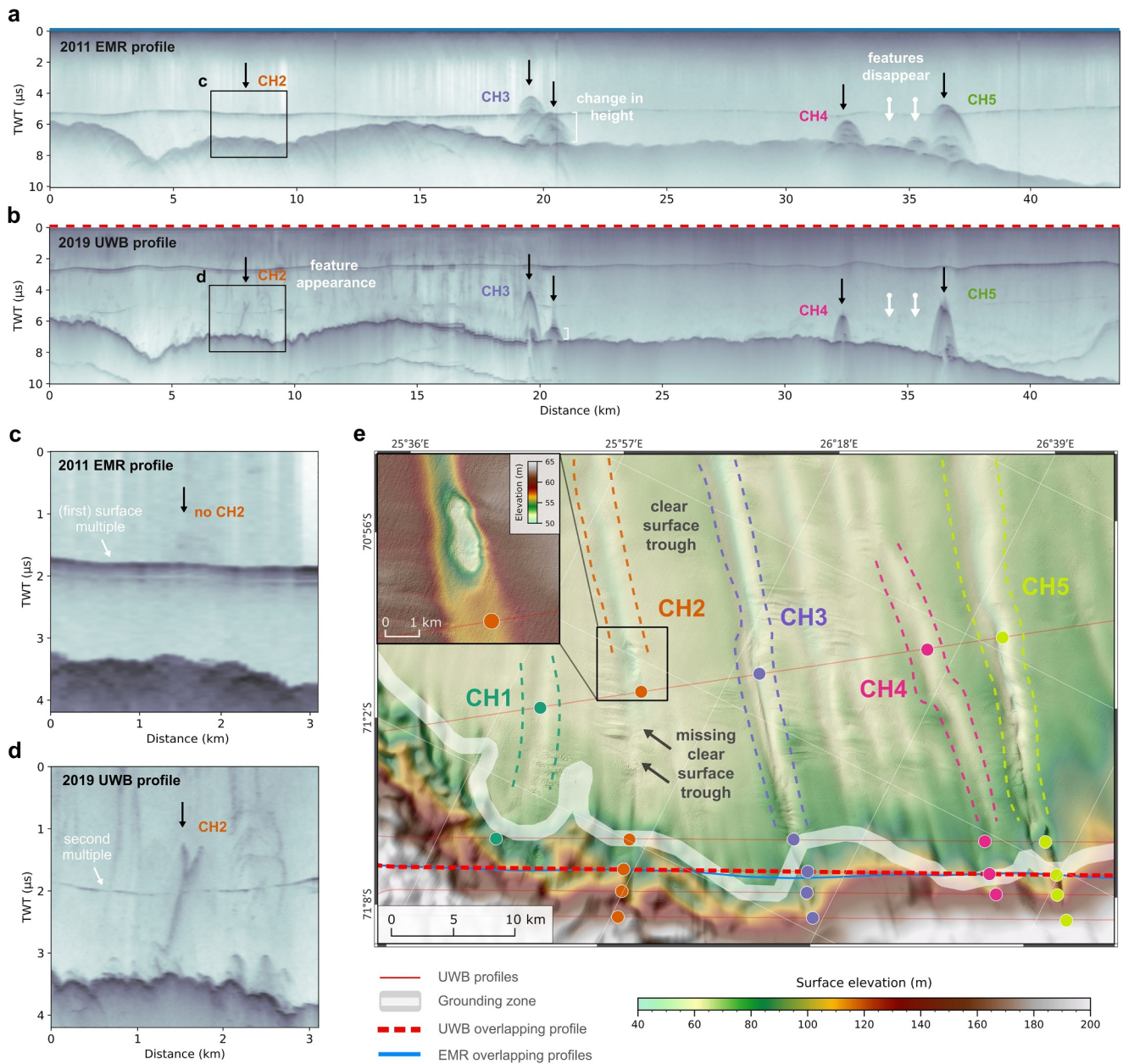


Figure 2. Temporal changes of englacial features near the grounding zone. (a) EMR Profile acquired in 2011 (profile 20113139), (b) UWB Profile acquired in 2019 (profile 20190106_01_004). Magnified views on englacial features at CH2 in the EMR and UWB profile are shown in (c) and (d). (e) Map view of ice-shelf surface features at locations where channels were detected in the radar data. The grounding zone (Mouginot et al., 2017) in (e) is indicated as a white band.

flux and basal friction, this input increases downstream due to faster ice flow and is largest in an area of thick ice that is grounded well below sea level (see -500 m bed elevation contour in Supplementary Figure S4 in Supporting Information S1). High water input in addition to high effective transmissivity then leads to high subglacial water flux toward the grounding zone that concentrates in the regions where we observe subglacial channels (Figure 3a). Considering solely the gradient of the hydropotential (which does not provide information on flow rates and water flow in channels), we note that at CH1, CH2, and CH3, the subglacial water precisely converges toward the detected channels (Figure 3b).

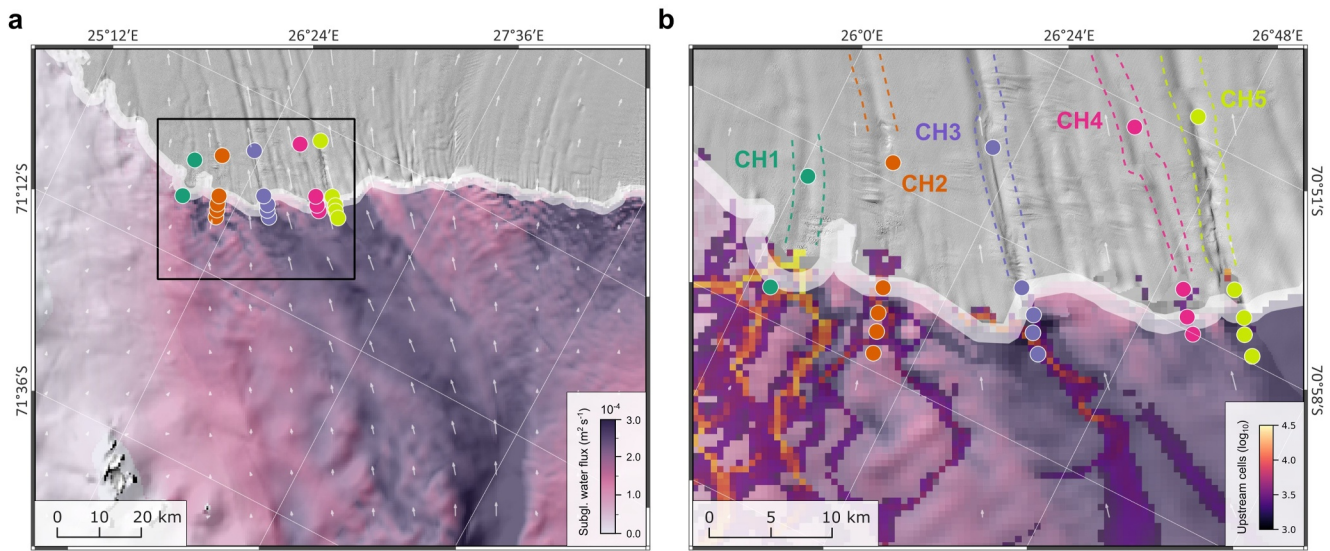


Figure 3. Overview of subglacial hydrological modeling, overlaid by the location (colored dots) of the channels in the radargrams (compare Figure 1b). (a) Subglacial water flux magnitude from CUAS-MPI. The white arrows indicate the direction of ice flow. (b) Magnified view of the survey region showing subglacial water routing (number of upstream cells) based on the hydropotential gradient. The grounding zone (Mouginot et al., 2017) is indicated as a white band.

4. Discussion

4.1. Temporal Dynamics of Subglacial Channel Activity

Our radar data documents five subglacial channels on the grounded ice sheet, intruding into the ice sheet and laterally extending into the Roi Baudoin Ice Shelf. Based on the available information, we cannot definitively determine whether the observed features are (a) completely water-filled cavities (Horgan et al., 2023; Whiteford et al., 2022) potentially filled with sediment (Drews et al., 2017), (b) smaller subglacial channels with vertical crevasses (Vaughan et al., 2012), or a combination of these possibilities. However, the combination of our radar observations, subglacial hydrological modeling, and features on the ice shelf, we consider it most likely that these are cavities probably filled with ocean water mixed with subglacial outflow.

The increase in size of the incision with decreasing distance to the grounding line remains consistent with observations at the grounding zone of the Kamb Ice Stream (Whiteford et al., 2022). Nonetheless, we note that the ice dynamic and topographic environment at the grounding zone of the Kamb Ice Stream is different from the setting at RBIS. However, so far little is known about temporal changes in subglacial channel activity. The geometry of the ice directly above the channels does not present a coherent pattern, as it appears as a mix of ridges, valleys, or flat topography (Figure 1c). Given our limited knowledge of the force balance within the channels and the fact that the channels seem relatively narrow (a few tens to hundreds of meters and thinning upstream), combined with the likelihood of a temporally varying water supply system and interactions with the ocean, a valley in the ice surface above the channels should not necessarily be expected.

Broadly speaking the locations of CH3–5 have remained stable in the time interval (2011–2019) given by our repeat radar transects, although some changes in the geometry of the ice-shelf cavity are evident. The stable locations are in line with the ice-shelf channel lineations further seawards, which appear near parallel to ice-shelf flow lines for hundreds of years of ice advection. CH2 (which was not evident in the 2011 EMR radar transect) has a distinctly different pattern in this regard because the corresponding ice-shelf channel extends far in the ice shelf but is disconnected to the contemporary grounding zone. This distance gap corresponds to approximately 60 years of ice advection.

We define “activity” in the sense that subglacial water is transported from the ice-sheet interior toward the grounding zone, creating Röthlisberger channels in a high-pressure system (Röthlisberger, 1972), potentially also combined with Nye channels (Nye, 1957), where it interacts with ocean water that primarily deepens and sustains the subglacial channel, and causes basal melting of the ice shelf in the direction of ice flow (Le Brocq et al., 2013;

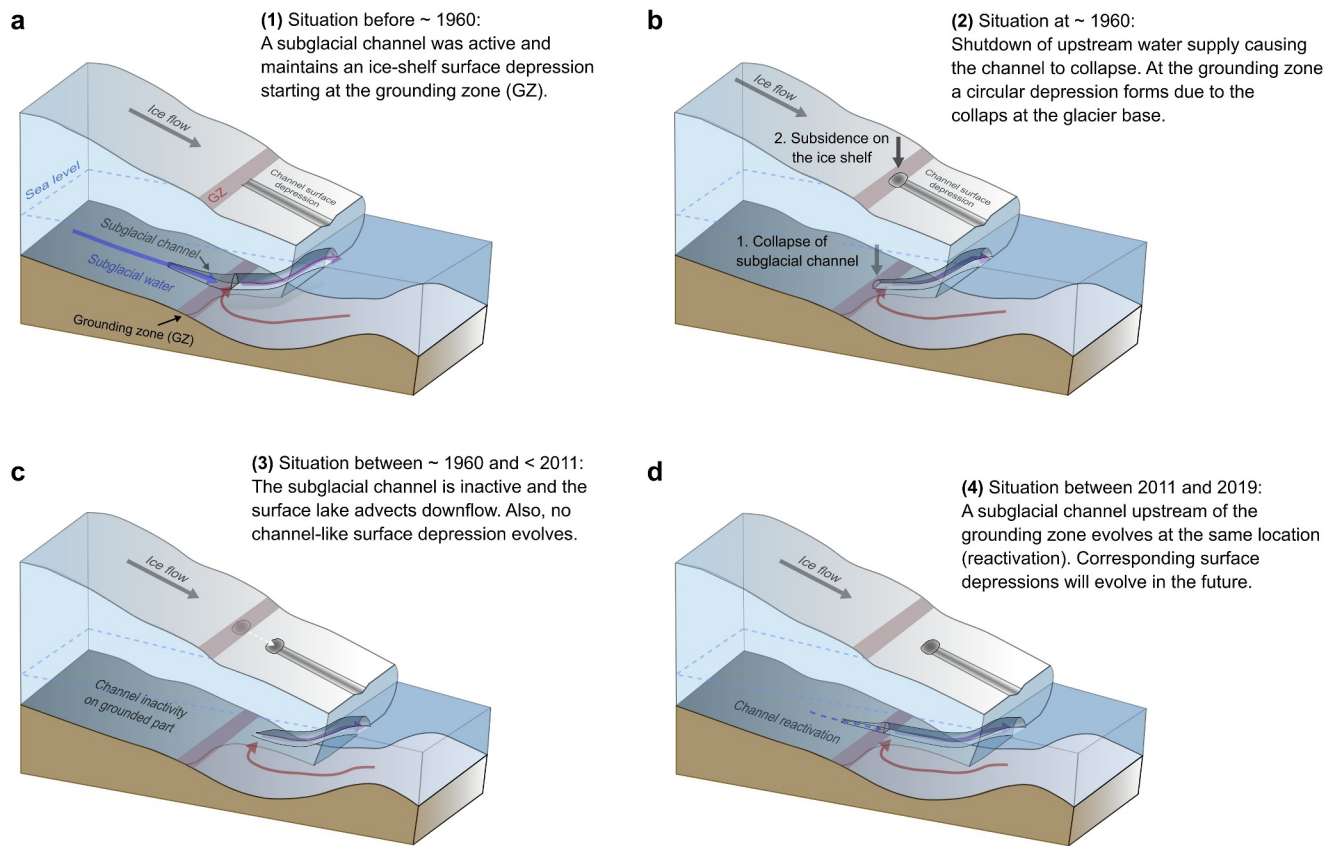


Figure 4. Sketch of the temporal evolution of subglacial channel activity at CH2 based on ice-surface and radar-feature interpretation.

Marsh et al., 2016; Rignot & Steffen, 2008). As soon as the combination of the water pressure, flux, and the contribution of ocean water can no longer maintain the subglacial channels open, the basal melting on the underside of the ice shelf also ceases, and with it, the basal channel signature at the ice shelf's surface (Alley et al., 2016).

Based on the radar and ice surface features associated with CH2 (Figure 2), we hypothesize the following temporal evolution scenario (summarized in Figure 4). (a) Subglacial channel CH2 was active many hundreds of years prior to ~1960 C.E. based on the current flow field and the trough extent on the ice shelf. Considering that we observe a clear ice surface trough up to a distance of ~5–10 km from the grounding zone along ice flow, the advection time corresponds to approximately 60 years with the present-day flow field. (b) The channel was deactivated around 1960 (60 years before the ice surface DEM date). We hypothesize that a substantial change of the subglacial characteristics caused a lowering at the ice surface and infill of supraglacial meltwater in a circular depression at the ice-shelf surface (Figure 2e). (c) As we observe no englacial reflection in our 2011 EMR data (Figure 2c), we suggest that the subglacial channel at CH2 remained inactive at least until 2011, that is, water flow and ocean water intrusion were too low to result in sufficiently high melt rates to cause incision of the channel into the ice-sheet base. (d) Between 2011 and 2019, the inland channel system of CH2 was reactivated, which we infer from characteristic englacial reflection in the 2019 UWB data (Figure 2d).

4.2. Potential Channel De- and Re-Activation Mechanisms

Our observations suggest that the subglacial hydrological system influences the subglacial channel location, and combined with direct interaction with the ocean, acts as the driving force behind the subglacial channels both on the grounded side as well as at the ice-shelf base. This is supported by our subglacial hydrological modeling and observations at other Antarctic grounding zones (Alley et al., 2016; Whiteford et al., 2022) and general modeling approaches (Lu & Kingslake, 2024). The system controls the location and melt rates at the ice underside on the

grounded channel as well as the melt rates of the plume. We consider two fundamental mechanisms that can lead to episodic changes in subglacial water supply at the same location:

If the subglacial hydrological system further upstream could predominantly be characterized as a distributed system, small changes in ice sheet geometry (top and base) will cause a shift in subglacial water flow. The water supply would thus follow the gradient of the hydropotential, which is most sensitive to gradients of the ice surface elevation. Possible explanations for changes in ice surface on timescales of less than 100 years could include changes in spatial snow accumulation patterns, changes in drainage geometry, or intense basal melting, resulting in relative lowering or raising of the ice surface or erosional and depositional sedimentary processes at the ice-sheet base. However, a mere relocation of water flow in the order required to make the ice-shelf imprints of CH2 disappear would have likely required another outlet feature to appear in the nearby environment.

Another possibility that could induce changes in channel activity is spatially fixed but temporary changes in water supply due to the filling and draining of subglacial lakes. Active subglacial lakes in this region have not been identified so far, but a large number of subglacial lakes and their network likely remain undiscovered (Neckel et al., 2021), with recent discoveries also made in this Antarctic sector (Arthur et al., 2024). The filling and draining of a subglacial lake would modulate melt rates and could thus explain the cessation and reactivation of subglacial channels at the same location.

The shutdown of subglacial channels near the grounding zone suggests a rapid and extensive change in the steady-state interaction between subglacial and ocean water. This could potentially have been caused by a subglacial flood (Marsh et al., 2016), resulting in extreme local melting and subsequent cessation of subglacial water supply. The consequences of such floods have recently been documented in a channel cavity on the Kamb ice stream (Kim et al., 2016; Whiteford et al., 2022). Especially in the context of the reactivation of the CH2 system, we consider substantial activity of a subglacial lake as reservoir for the subglacial water supply on time scales of decades instead of an overall shift in the subglacial hydrological system as more plausible.

4.3. Significance for the Antarctic Ice-Shelf System

The flow of substantial volumes of freshwater from subglacial hydrological channels into ice-shelf cavities has been demonstrated to play a crucial role in basal melting of ice shelves at the grounding zone (Dow et al., 2022; Wei et al., 2020). Subglacial water flux from the inland alone cannot create and sustain the observed hundred-meters high subglacial channels observed here. Nonetheless, we find strong indications, that it impacts the initiation and evolution of basal channels, in turn affecting ice-shelf stability, and the occurrence of calving events (Dow et al., 2018). Moreover, subglacial channels imprint changes in ocean and atmospheric forcings at the ice-shelf surface (Alley et al., 2024; Drews et al., 2020). Our observation of the transient behavior of channels upstream of and at the grounding zone over timescales of decades makes it even more challenging to project their impact on Antarctica's ice-shelf systems in the future and their contribution to the vulnerability to grounding zone retreat (Chartrand et al., 2024; Lu & Kingslake, 2024; Rignot et al., 2024). It highlights the need for fully coupled ice-sheet-hydrology simulations as (re-)activation of channels can trigger ocean plumes at the grounding zone, and their deactivation can also cease or weaken the interaction with the ocean. Such processes thus also influence ice-shelf thinning and thickening and the interaction of the ice shelf with pinning points (Berger et al., 2017; Whiteford et al., 2022).

5. Conclusions

Subglacial signatures from repeated radar measurements and morphological features on the ice-shelf surface near the grounding zone between the West Ragnhild Glacier and Roi Baudouin Ice Shelf in East Antarctica reveal temporal changes in the subglacial hydrological system. We inferred that subglacial channels can shut down and reactivate at the same location around the grounding zones within decades, indicating an interaction between subglacial water supply and ocean water intrusion undergoing episodic phases of activity and shut down. These are potentially more likely linked to the filling and draining of subglacial lakes than the relocation of water routing due to ice-sheet geometry changes, as well as changes in ocean plumes, although we do not have evidence which process prevails and causes the temporal change. Variability on such short timescales has not been observed in this region before, providing new insights into the transient nature of the subglacial system around the grounding zone of the Antarctic Ice Sheet, which profoundly affects ice-shelf–ocean processes. A better understanding of these temporal changes in the hydrological system incorporating lake drainage mechanisms is necessary to

understand the associated physical mechanisms better, yet at the same time presents significant challenges for simulating such processes and thus increases uncertainties in future predictions of processes related to subglacial hydrology.

Data Availability Statement

Radar data products from the AWI UWB CHIRP survey in the 2018/19 season (Franke et al., 2023) and from the AWI EMR survey in the 2010/11 season (Jokat et al., 2024) are available on the PANGAEA data repository. The CUAS simulation output is available at Zenodo (Kleiner & Humbert, 2024). The REMA ice surface DEM (Howat et al., 2022) is available from the U.S. Polar Geospatial Center. BedMachine Antarctica (Version 3; Morlighem et al., 2020) and ice surface flow velocities from Mouginot et al. (2019) are available at the National Snow and Ice Data Center. CUAS-MPI is available at <https://github.com/tudasc/CUAS-MPI>.

Acknowledgments

Logistical support was provided at Princess Elisabeth Station (Belgium), Troll Station (Norway) and Novolazarevskaja Station (Russia). Airborne radar data were acquired in austral summer 2018/19 by the Alfred Wegener Institute Helmholtz Centre for Polar and Marine Research (AWI) within the CHIRP project (AWI Grant ID: AWI_PA_02106). The 2010/11 survey was funded by the European Facilities for Airborne Research (EUFAR). We thank the Kenn Borek crew as well as Martin Gehrmann and Sebastian Spelz of AWI's technical staff of the research aircraft Polar 6. Furthermore, we thank John Paden, Tobias Binder, Daniel Steinhage and Veit Helm for supporting data acquisition and processing. We acknowledge the use of software from Open Polar Radar generated with support from the University of Kansas, NASA grants 80NSSC20K1242 and 80NSSC21K0753, and NSF grants OPP-2027615, OPP-2019719, OPP-1739003, IIS-1838230, RISE-2126503, RISE-2127606, and RISE-2126468. The authors would like to thank Aspen Technology, Inc. for providing software licenses and support. Yan Zhou acknowledges financial support from the China Scholarship Council (CSC File No. 202106170106) for his research stay at AWI. Steven Franke was funded by the Walter Benjamin Programme of the Deutsche Forschungsgemeinschaft (DFG, German Research Foundation; project number 506043073). Reinhard Drews was supported by an Emmy Noether Grant of the Deutsche Forschungsgemeinschaft (DR 822/3–1). We thank Michael Wolovick for providing the ice-sheet basal melt data set used for the CUAS-MPI simulations. Moreover, we thank the editor Mathieu Morlighem as well as Neil Ross and another anonymous reviewer for their helpful suggestions, which greatly improved the manuscript. Open Access funding enabled and organized by Projekt DEAL.

References

- Alfred-Wegener-Institut Helmholtz-Zentrum für Polar- und Meeresforschung. (2016). Polar aircraft Polar5 and Polar6 operated by the Alfred Wegener Institute. *Journal of Large-Scale Research Facilities JLSRF*, 2, A87. <https://doi.org/10.17815/jlsrf-2-153>
- Alley, K. E., Alley, R. B., Crawford, A. D., Ochwat, N., Wild, C. T., Marson, J., et al. (2024). Evolution of sub-ice-shelf channels reveals changes in ocean-driven melt in West Antarctica. *Journal of Glaciology*, 70, 1–15. <https://doi.org/10.1017/jog.2024.20>
- Alley, K. E., Scambos, T. A., Siegfried, M. R., & Fricker, H. A. (2016). Impacts of warm water on Antarctic ice shelf stability through basal channel formation. *Nature Geoscience*, 9(4), 290–293. <https://doi.org/10.1038/ngeo2675>
- Arthur, J. F., Shackleton, C., Moholdt, G., Matsuoka, K., & Oostveen, J. v. (2024). Evidence of active subglacial lakes under a slowly moving coastal region of the Antarctic Ice Sheet. *EGU sphere*, 2024, 1–28. <https://doi.org/10.5194/egusphere-2024-1704>
- Berger, S., Drews, R., Helm, V., Sun, S., & Pattyn, F. (2017). Detecting high spatial variability of ice shelf basal mass balance, Roi Baudouin Ice Shelf, Antarctica. *The Cryosphere*, 11(6), 2675–2690. <https://doi.org/10.5194/tc-11-2675-2017>
- Beyer, S. (2020). Cordial drainage routing engine (CiDRE) v1. <https://gitlab.com/sebastianbeyer/CiDRE.gitlab>
- Beyer, S., Kleiner, T., Aizinger, V., Rückamp, M., & Humbert, A. (2018). A confined–unconfined aquifer model for subglacial hydrology and its application to the Northeast Greenland Ice Stream. *The Cryosphere*, 12(12), 3931–3947. <https://doi.org/10.5194/tc-12-3931-2018>
- Callens, D., Matsuoka, K., Steinhage, D., Smith, B., Witrant, E., & Pattyn, F. (2014). Transition of flow regime along a marine-terminating outlet glacier in East Antarctica. *The Cryosphere*, 8(3), 867–875. <https://doi.org/10.5194/tc-8-867-2014>
- Chartrand, A. M., Howat, I. M., Joughin, I. R., & Smith, B. E. (2024). Thwaites Glacier thins and retreats fastest where ice-shelf channels intersect its grounding zone. *The Cryosphere*, 18(11), 4971–4992. <https://doi.org/10.5194/tc-18-4971-2024>
- Cheng, C., Jenkins, A., Holland, P. R., Wang, Z., Dong, J., & Liu, C. (2024). Ice shelf basal channel shape determines channelized ice-ocean interactions. *Nature Communications*, 15(1), 2877. <https://doi.org/10.1038/s41467-024-47351-z>
- de Fleurian, B., Morlighem, M., Seroussi, H., Rignot, E., van den Broeke, M. R., Kuipers Munneke, P., et al. (2016). A modeling study of the effect of runoff variability on the effective pressure beneath Russell Glacier, West Greenland. *Journal of Geophysical Research: Earth Surface*, 121(10), 1834–1848. <https://doi.org/10.1002/2016JF003842>
- Dow, C. F., Lee, W. S., Greenbaum, J. S., Greene, C. A., Blankenship, D. D., Poinar, K., et al. (2018). Basal channels drive active surface hydrology and transverse ice shelf fracture. *Science Advances*, 4(6), eaao7212. <https://doi.org/10.1126/sciadv.aao7212>
- Dow, C. F., Ross, N., Jeffroy, H., Siu, K., & Siegert, M. J. (2022). Antarctic basal environment shaped by high-pressure flow through a subglacial river system. *Nature Geoscience*, 15(11), 892–898. <https://doi.org/10.1038/s41561-022-01059-1>
- Drews, R. (2015). Evolution of ice-shelf channels in Antarctic ice shelves. *The Cryosphere*, 9(3), 1169–1181. <https://doi.org/10.5194/tc-9-1169-2015>
- Drews, R., Pattyn, F., Hewitt, I. J., Ng, F. S. L., Berger, S., Matsuoka, K., et al. (2017). Actively evolving subglacial conduits and eskers initiate ice shelf channels at an Antarctic grounding line. *Nature Communications*, 8(15228), 15228. <https://doi.org/10.1038/ncomms15228>
- Drews, R., Schannwell, C., Ehlers, T. A., Gladstone, R., Pattyn, F., & Matsuoka, K. (2020). Atmospheric and oceanographic signatures in the ice shelf channel morphology of Roi Baudouin Ice Shelf, East Antarctica, inferred from radar data. *Journal of Geophysical Research: Earth Surface*, 125(7), e2020JF005587. <https://doi.org/10.1029/2020JF005587>
- Dupont, T. K., & Alley, R. B. (2005). Assessment of the importance of ice-shelf buttressing to ice-sheet flow. *Geophysical Research Letters*, 32(4). <https://doi.org/10.1029/2004gl022024>
- Edwards, T. L., Nowicki, S., Marzeion, B., Hock, R., Goelzer, H., Seroussi, H., et al. (2021). Projected land ice contributions to twenty-first-century sea level rise. *Nature*, 593(7857), 74–82. <https://doi.org/10.1038/s41586-021-03302-y>
- Favier, L., Pattyn, F., Berger, S., & Drews, R. (2016). Dynamic influence of pinning points on marine ice-sheet stability: A numerical study in Dronning Maud Land, East Antarctica. *The Cryosphere*, 10(6), 2623–2635. <https://doi.org/10.5194/tc-10-2623-2016>
- Fischler, Y., Kleiner, T., Bischof, C., Schmiedel, J., Sayag, R., Emunds, R., et al. (2023). A parallel implementation of the confined–unconfined aquifer system model for subglacial hydrology: Design, verification, and performance analysis (CUAS-MPI v0.1.0). *Geoscientific Model Development*, 16(18), 5305–5322. <https://doi.org/10.5194/gmd-16-5305-2023>
- Fox, D. (2023). A massive cavern beneath a West Antarctic glacier is teeming with life. *Science News*. Retrieved from <https://www.sciencenews.org/article/cavern-west-antarctic-glacier-life>
- Franke, S., Eisermann, H., Jokat, W., Eagles, G., Asseng, J., Miller, H., et al. (2021). Preserved landscapes underneath the Antarctic ice sheet reveal the geomorphological history of Jutulstraumen Basin. *Earth Surface Processes and Landforms*, 46(13), 2728–2745. <https://doi.org/10.1002/esp.5203>
- Franke, S., Jansen, D., Binder, T., Paden, J. D., Dörr, N., Gerber, T. A., et al. (2022). Airborne ultra-wideband radar sounding over the shear margins and along flow lines at the onset region of the Northeast Greenland Ice Stream. *Earth System Science Data*, 14(2), 763–779. <https://doi.org/10.5194/essd-14-763-2022>
- Franke, S., Jansen, D., Drews, R., Steinhage, D., Helm, V., & Eisen, O. (2023). Ultra-wideband radar data over the ice shelves and ice rises in eastern Dronning Maud Land (East Antarctica) [Dataset]. PANGAEA. <https://doi.org/10.1594/PANGAEA.963264>

- Fürst, J. J., Durand, G., Gillet-Chaulet, F., Tavard, L., Rankl, M., Braun, M., & Gagliardini, O. (2016). The safety band of Antarctic ice shelves. *Nature Climate Change*, 6(5), 479–482. <https://doi.org/10.1038/nclimate2912>
- Gourmelen, N., Goldberg, D. N., Snow, K., Henley, S. F., Bingham, R. G., Kimura, S., et al. (2017). Channelized melting drives thinning under a rapidly melting Antarctic ice shelf. *Geophysical Research Letters*, 44(19), 9796–9804. <https://doi.org/10.1002/2017GL074929>
- Hale, R., Miller, H., Gogineni, S., Yan, J. B., Rodriguez-Morales, F., Leuschen, C., et al. (2016). Multi-channel ultra-wideband radar sounder and imager. 2016 IEEE International Geoscience and Remote Sensing Symposium (IGARSS), 2112–2115. <https://doi.org/10.1109/IGARSS.2016.7729545>
- Holland, P. R., Feltham, D. L., & Jenkins, A. (2007). Ice shelf water plume flow beneath Filchner-Ronne Ice Shelf, Antarctica. *Journal of Geophysical Research*, 112(C5). <https://doi.org/10.1029/2006jc003915>
- Horgan, H., Dunbar, G., Hulbe, C., Schmidt, B., Stevens, C., Stewart, C., & the KIS2 Science Team. (2023). Subglacial drainage across Kamb ice stream's grounding zone, west Antarctica. In *EGU General Assembly 2023, Vienna, Austria, 24–28 Apr 2023. (EGU23-1820)*. <https://doi.org/10.5194/egusphere-egu23-1820>
- Howat, I., Porter, C., Noh, M.-J., Husby, E., Khuvis, S., Danish, E., et al. (2022). The reference elevation model of Antarctica - Mosaics, version 2. *Harvard Dataverse*. <https://doi.org/10.7910/DVN/EBW8UC>
- Howat, I., Porter, C., Smith, B. E., Noh, M.-J., & Morin, P. (2019). The reference elevation model of Antarctica. *The Cryosphere*, 13(2), 665–674. <https://doi.org/10.5194/tc-13-665-2019>
- Humbert, A., Christmann, J., Corr, H. F. J., Helm, V., Höyns, L.-S., Hofstede, C., et al. (2022). On the evolution of an ice shelf melt channel at the base of Filchner Ice Shelf, from observations and viscoelastic modeling. *The Cryosphere*, 16(10), 4107–4139. <https://doi.org/10.5194/tc-16-4107-2022>
- Jacobel, R. W., Christianson, K., Wood, A. C., Dallasanta, K. J., & Gobel, R. M. (2014). Morphology of basal crevasses at the grounding zone of Whillans Ice Stream, West Antarctica. *Annals of Glaciology*, 55(67), 57–63. <https://doi.org/10.3189/2014aog67a004>
- Jenkins, A. (1991). A one-dimensional model of ice shelf-ocean interaction. *Journal of Geophysical Research*, 96(C11), 20671–20677. <https://doi.org/10.1029/91jc01842>
- Jeofry, H., Ross, N., Le Brocq, A., Graham, A. G., Li, J., Gogineni, P., et al. (2018). Hard rock landforms generate 130 km ice shelf channels through water focusing in basal corrugations. *Nature Communications*, 9(1), 4576. <https://doi.org/10.1038/s41467-018-06679-z>
- Jokat, W., Steinhage, D., & Helm, V. (2024). Ant 2010/11: AWI airborne radio-echo sounding data over central east Antarctica connecting the EDML and South Pole ice core (WEGAS project) [Dataset]. *PANGAEA*. <https://doi.pangaea.de/10.1594/PANGAEA.974319>
- Kamb, B. (1987). Glacier surge mechanism based on linked cavity configuration of the basal water conduit system. *Journal of Geophysical Research*, 92(B9), 9083–9100. <https://doi.org/10.1029/JB092iB09p09083>
- Kim, B.-H., Lee, C.-K., Seo, K.-W., Lee, W. S., & Scambos, T. (2016). Active subglacial lakes and channelized water flow beneath the Kamb Ice Stream. *The Cryosphere*, 10(6), 2971–2980. <https://doi.org/10.5194/tc-10-2971-2016>
- Kleiner, T., & Humbert, A. (2024). CUAS-MPI subglacial hydrology as used in Zhou et al., Geophysical Research Letters [Dataset]. *Zenodo*. <https://doi.org/10.5281/zenodo.14531376>
- Koch, I., Drews, R., Franke, S., Jansen, D., Oraschewski, F. M., Muhle, L. S., et al. (2023). Radar internal reflection horizons from multisystem data reflect ice dynamic and surface accumulation history along the Princess Ragnhild Coast, Dronning Maud Land, East Antarctica. *Journal of Glaciology*, 70, 1–19. <https://doi.org/10.1017/jog.2023.93>
- Le Brocq, A. M., Ross, N., Griggs, J. A., Bingham, R. G., Corr, H. F. J., Ferraccioli, F., et al. (2013). Evidence from ice shelves for channelized meltwater flow beneath the Antarctic Ice Sheet. *Nature Geoscience*, 6(11), 945–948. <https://doi.org/10.1038/ngeo1977>
- Lenaerts, J. T. M., Lhermitte, S., Drews, R., Ligtenberg, S. R. M., Berger, S., Helm, V., et al. (2017). Meltwater produced by wind-albedo interaction stored in an East Antarctic ice shelf. *Nature Climate Change*, 7(1), 58–62. <https://doi.org/10.1038/nclimate3180>
- Leuschen, C., Gogineni, S., & Tammana, D. (2000). Sar processing of radar echo sounder data. IGARSS 2000. IEEE 2000 International geoscience and remote sensing symposium. Taking the pulse of the planet: The role of remote sensing in managing the environment. *Proceedings*, 6, 2570–2572. <https://doi.org/10.1109/IGARSS.2000.859643>
- Lu, G., & Kingslake, J. (2024). Two-way coupling between ice flow and channelized subglacial drainage enhances modeled marine-ice-sheet retreat. *The Cryosphere*, 18(11), 5301–5321. <https://doi.org/10.5194/tc-18-5301-2024>
- Marsh, O. J., Fricker, H. A., Siegfried, M. R., Christianson, K., Nicholls, K. W., Corr, H. F. J., & Catania, G. (2016). High basal melting forming a channel at the grounding line of Ross Ice Shelf, Antarctica. *Geophysical Research Letters*, 43(1), 250–255. <https://doi.org/10.1002/2015GL066612>
- Morlighem, M., Rignot, E., Binder, T., Blankenship, D., Drews, R., Eagles, G., et al. (2020). Deep glacial troughs and stabilizing ridges unveiled beneath the margins of the Antarctic Ice Sheet. *Nature Geoscience*, 13(2), 132–137. <https://doi.org/10.1038/s41561-019-0510-8>
- Mouginot, J., Rignot, E., & Scheuchl, B. (2019). Continent-wide, interferometric SAR phase, mapping of Antarctic ice velocity. *Geophysical Research Letters*, 46(16), 9710–9718. <https://doi.org/10.1029/2019gl083826>
- Mouginot, J., Scheuchl, B., & Rignot, E. (2017). MEaSURES Antarctic boundaries for IPY 2007–2009 from satellite radar. <https://doi.org/10.5067/AXE4121732AD>
- Neckel, N., Franke, S., Helm, V., Drews, R., & Jansen, D. (2021). Evidence of cascading subglacial water flow at Jutulstraumen Glacier (Antarctica) derived from Sentinel-1 and ICESat-2 measurements. *Geophysical Research Letters*, 48(20). <https://doi.org/10.1029/2021gl094472>
- Nixdorf, U., Steinhage, D., Meyer, U., Hempel, L., Jenett, M., Wachs, P., & Miller, H. (1999). The newly developed airborne radio-echo sounding system of the AWI as a glaciological tool. *Annals of Glaciology*, 29, 231–238. <https://doi.org/10.3189/172756499781821346>
- Nye, J. F. (1957). The distribution of stress and velocity in glaciers and ice-sheets. *Proceedings of the Royal Society of London, Series A: Mathematical and Physical Sciences*, 239(1216), 113–133. <https://doi.org/10.1098/rspa.1957.0026>
- Nye, J. F. (1976). Water flow in glaciers: Jökulhlaups, tunnels and veins. *Journal of Glaciology*, 17(76), 181–207. <https://doi.org/10.3189/S002214300001354X>
- Open Polar Radar. (2023). Open polar radar. Opr (version 3.0.1) [Computer software]. <https://doi.org/10.5281/zenodo.5683959>
- Parizek, B. R. (2024). Grounding zones: The “inland” dynamic interface between seawater, outlet glaciers, subglacial meltwater routing, and ice-shelf processes. *Geophysical Research Letters*, 51(15), e2024GL110427. <https://doi.org/10.1029/2024GL110427>
- Reese, R., Gudmundsson, G. H., Levermann, A., & Winkelmann, R. (2018). The far reach of ice-shelf thinning in Antarctica. *Nature Climate Change*, 8(1), 53–57. <https://doi.org/10.1038/s41558-017-0020-x>
- Rignot, E., Ciraci, E., Scheuchl, B., Tolpekin, V., Wollersheim, M., & Dow, C. (2024). Widespread seawater intrusions beneath the grounded ice of Thwaites Glacier, West Antarctica. *Proceedings of the National Academy of Sciences*, 121(22), e2404766121. <https://doi.org/10.1073/pnas.2404766121>

- Rignot, E., & Steffen, K. (2008). Channelized bottom melting and stability of floating ice shelves. *Geophysical Research Letters*, *35*(2). <https://doi.org/10.1029/2007gl031765>
- Rodríguez-Morales, F., Byers, K., Crowe, R., Player, K., Hale, R. D., Arnold, E. J., et al. (2014). Advanced multifrequency radar instrumentation for polar research. *IEEE Transactions on Geoscience and Remote Sensing*, *52*(5), 2824–2842. <https://doi.org/10.1109/tgrs.2013.2266415>
- Röthlisberger, H. (1972). Water pressure in intra- and subglacial channels. *Journal of Glaciology*, *11*(62), 177–203. <https://doi.org/10.1017/S0022143000022188>
- Schwanghart, W., & Kuhn, N. J. (2010). Topotoolbox: A set of Matlab functions for topographic analysis. *Environmental Modelling and Software*, *25*(6), 770–781. <https://doi.org/10.1016/j.envsoft.2009.12.002>
- Shreve, R. L. (1972). Movement of water in glaciers. *Journal of Glaciology*, *11*(62), 205–214. <https://doi.org/10.3189/S002214300002219X>
- van der Linden, E. C., Le Bars, D., Lambert, E., & Drijfhout, S. (2023). Antarctic contribution to future sea level from ice shelf basal melt as constrained by ice discharge observations. *The Cryosphere*, *17*(1), 79–103. <https://doi.org/10.5194/tc-17-79-2023>
- Vaughan, D. G., Corr, H. F. J., Bindschadler, R. A., Dutrieux, P., Gudmundsson, G. H., Jenkins, A., et al. (2012). Subglacial melt channels and fracture in the floating part of Pine Island Glacier, Antarctica. *Journal of Geophysical Research*, *117*(F3). <https://doi.org/10.1029/2012JF002360>
- Walder, J. S. (1986). Hydraulics of subglacial cavities. *Journal of Glaciology*, *32*(112), 439–445. <https://doi.org/10.3189/S0022143000012156>
- Wei, W., Blankenship, D. D., Greenbaum, J. S., Gourmelen, N., Dow, C. F., Richter, T. G., et al. (2020). Getz ice shelf melt enhanced by freshwater discharge from beneath the West Antarctic Ice Sheet. *The Cryosphere*, *14*(4), 1399–1408. <https://doi.org/10.5194/tc-14-1399-2020>
- Werder, M. A., Hewitt, I. J., Schoof, C. G., & Flowers, G. E. (2013). Modeling channelized and distributed subglacial drainage in two dimensions. *Journal of Geophysical Research: Earth Surface*, *118*(4), 2140–2158. <https://doi.org/10.1002/jgrf.20146>
- Whiteford, A., Horgan, H. J., Leong, W. J., & Forbes, M. (2022). Melting and refreezing in an ice shelf basal channel at the grounding line of the Kamb ice stream, west Antarctica. *Journal of Geophysical Research: Earth Surface*, *127*(11), e2021JF006532. <https://doi.org/10.1029/2021JF006532>
- Zhang, Y., Sachau, T., Franke, S., Yang, H., Li, D., Weikusat, I., & Bons, P. D. (2024). Formation mechanisms of large-scale folding in Greenland's ice sheet. *Geophysical Research Letters*, *51*(16). <https://doi.org/10.1029/2024gl1109492>